Combined Optical and Radio-Frequency Perspectives on the Time Evolution of Lightning Measured by the FORTE Satellite

Michael Peterson[1]

[1]ISR-2, Los Alamos National Laboratory, Los Alamos, New Mexico

Corresponding author: Michael Peterson (mpeterson@lanl.gov), B241, P.O. Box 1663 Los Alamos, NM, 87545

Key Points:

- The FORTE satellite provided coincident lightning measurements from a lightning imager, a photodiode detector, and VHF-band RF sensors
- Joint observations reveal that wide-FOV optical and RF detectors routinely capture flash activity that is missed by the pixelated imager
- Current and future space-based missions that use wide-FOV instruments might resolve flash details that are missed by OTD / LIS / GLM

LA-UR-22-20053

Abstract

We use a cluster feature dataset for the Fast On-orbit Recording of Transient Events (FORTE) satellite that combines detections from its pixelated lightning imager (Lightning Locating System: LLS), photodiode detector (PDD) and Radio-Frequency (RF) instrumentation to generate statistics describing the frequency and timing of lightning events detected by each instrument during lightning flashes. Coincident observations from the same vantage point allow us to directly compare flash details that can be resolved by the wide Field of View (FOV) instruments relative to the pixelated LLS – whose design is based on NASA's Lightning Imaging Sensor (LIS).

We find that both the PDD and RF system typically generate more detections than the lightning imager (mean: 1.5 PDD events per LLS group, 2 RF events per LLS group) from pulses that are either not sufficiently bright in the optical band (in the case of RF) or that lack the optical energy density (in the case of the PDD) required to trigger one of the pixels on the LLS imaging array. This includes additional activity before the first LLS group or after the final LLS group.

These FORTE results demonstrate that certain lightning processes would be better resolved by wide-FOV optical and RF instruments than lightning imagers. Current / future space-based missions that use / plan to use similar instruments will improve our understanding of flash evolution by resolving details missed by lightning imagers.

Plain Language Summary

Our interpretation of how a lightning flash evolves is limited by how much of its development we can sense. Combining individual measurements of the same lightning taken by instruments that sense different aspects of its development can provide a comprehensive view of flash evolution. The Fast On-orbit Recording of Transient Events (FORTE) satellite contained three different types of lightning sensors that each measured lightning in a different way: a slower optical pixelated lightning imager, a faster photodiode detector, and a set of Radio Frequency instrumentation.

In this study, we compare how the pictures of lightning development differ between the instruments on FORTE – with a particular focus placed on the differences between the wide Field of View sensors (PDD, RF) and the lightning imager that is comparable to NASA's Lightning Imaging Sensor (LIS) and NOAA's Geostationary Lightning Mapper (GLM). We find that the wide-FOV instruments typically detect more lightning activity from the same set of flashes (often, before the first LLS detection). Thus, instruments like the PDD and RF system on FORTE (and similar instrumentation on future space-based missions) can provide additional context on how flashes evolve over time beyond the LIS / GLM analyses that are common today.

1 Introduction

While the question of "what defines a lighting flash" remains a topic of theoretical discussion, individual lightning sensors must make practical distinctions between lightning activity that clearly comprises separate electrical discharges within the cloud (Cummins et al., 1998; Murphy and Nag, 2015; Mach et al., 2007; Mach, 2020; Fuchs et al., 2016). Each instrument's perspective on what defines a lightning flash depends on what processes in the flash it can sense, and how flashes are constructed from its data. Lightning sensors that locate sub-flash components generally consider temporal and geospatial proximity to delineate individual flashes. Lightning develops in a particularly way, as an expanding network of hot plasma channels, and there are limits to this type of development (Rakov, 2007; Hill et al., 2011; Campos et al., 2014; van der Velde et al., 2013). If new activity is noted far from the existing structure of the developing flash with no points in-between, then it is probably not connected to the existing lightning channels, and represents a separate discharge.

NASA's Lightning Imaging Sensors (LIS: Christian et al., 2000; Blakeslee et al., 2020) and NOAA's Geostationary Lightning Mapper (GLM: Goodman et al., 2013; Rudlosky et al., 2019) observe the optical emissions along these lightning channels from space, and have proven valuable for mapping lightning development from orbit (Peterson et al., 2017a; 2018). Both instruments have identified cases of long horizontal "megaflashes" (Lyons et al., 2020; Peterson, 2021a; Peterson and Stano, 2021) that can extend over hundreds of kilometers (Peterson et al., 2019). However, the LIS / GLM view of these megaflashes usually starts at the rear of the convective thunderstorm core as the flashes begin to propagate into the stratiform region. Ground-based Lightning Mapping Array (LMA: Rison et al,. 1999) observations of similar megaflashes show a continued development that starts within the convective core before

86 developing into the stratiform region (Lang et al., 2017).

87 These megaflash cases demonstrate that the space-based lightning imager measurements
88 provided by LIS, GLM, and other instruments, while important, are prone to missing certain
89 types of flash development that are apparent to other instruments. Even though LIS / GLM
90 spatio-temporal clustering has been shown to be robust (i.e., Mach et al., 2007; Mach, 2020), if
91 the instrument senses no events from a portion the flash, then there is nothing to cluster and the
92 LIS / GLM picture of what defines a lightning flash is incomplete. Previous comparisons
93 between LIS and an LMA showed that LIS tended to trigger late in the discharge (Thomas et al.,
94 2000), and this is also why we consider the recently-certified new lightning extreme (Peterson et
95 al., 2020) for flash extent (709 km, as measured by GLM) to be a minimum estimate for the size
96 of this truly-exceptional flash that more than doubled the previous LMA-based record, rather
97 than its actual size.

98 There are a number of scenarios that can lead to a space-based lightning imager like
99 GLM missing activity within the flash. Certain lightning phenomena including Narrow Bipolar
100 Events (NBEs: Smith et al., 1999; Eack, 2004; Rison et al., 2016) are “dark” to GLM’s narrow
101 spectral band at 777.4 nm (Jacobson et al., 2002; Light et al., 2002), but can be seen in the 337
102 nm optical band (Soler et al., 2020) and are some of the strongest natural emitters in the Very
103 High Frequency (VHF) band in the Radio-Frequency (RF) spectrum (LeVine, 1980). Even in
104 cases where there is strong emission in GLM’s band, the emitter might not be bright enough to
105 trigger the instrument. The amount of optical energy radiated by lightning depends on the
106 amount of current flowing through the channel and the length of the channel that is active during
107 the discharge (Guo and Krider, 1982; Idone and Orville, 1985; Wang et al., 2005; Qie et al.,
108 2011; Carvalho et al., 2015; Quick et al., 2017). Initial flash development is at a disadvantage for

producing bright optical pulses due to the small overall channel lengths. These optical emissions are then released into the surrounding cloud medium, which modifies them through scattering and absorption (Thomson and Krider, 1982; Koshak et al., 1994; Light et al., 2001a; Suszcynsky et al., 2000; Brunner and Bitzer, 2020; Peterson, 2020,2021b). Scattering causes the photons to be redistributed throughout the cloud scene with their paths to the satellite determined by the geometry and composition of the surrounding clouds. The amount of absorption and the scattering time delay experienced by the signals that make it to the satellite depend on the paths taken by the photons through the cloud (i.e., the total path length and the number of scattering interactions along the path). We have observed and modeled cases of optical lightning emissions taking "shortcut" paths to the satellite by escaping through a nearby cloud boundary and reflecting off the edges of neighboring clouds to reach the satellite (Peterson, 2020; Peterson and Liu, 2013; Peterson et al., 2017a,b), and also cases of particularly-dense clouds preventing detection entirely (Peterson and Liu, 2013; Peterson, 2021b). LIS detection of LMA sources has also been shown to drop off below 10-km altitude due to increased cloud mass above the illuminated lightning channels (Thomas et al., 2000), and dense convective clouds are considered a primary cause of poor GLM performance in certain types of storms (i.e., Bitzer, 2019; Said and Murphy, 2019; Thomas, 2019; Rutledge et al., 2019).

However, even when the emissions make it to the cloud-top, they might not result in a detection by a lightning imager like GLM. These instruments record the total optical energy in each pixel on its imaging array, subtract the estimated background energy from the scene, and then compare the remaining energy to a local threshold value (Christian et al., 2000; Goodman et al., 2013). An "event" is only declared in any of these pixels if the signal exceeds this threshold value. This creates multiple scenarios where the instrument might fail to trigger on certain types

of lightning pulses. If the emitter is weak to begin with, or subject to severe attenuation in the cloud medium, or the local GLM threshold happens to be particularly high, then the optical signals that reach the satellite will be too dim to detect. Alternatively, weak emissions along a long horizontal channel, or low-altitude emissions that have been severely broadened geospatially by scattering in the cloud, or emissions from sources that happen to be located at GLM pixel boundaries as discussed in Zhang et al., (2020) will have their total optical energy divided between multiple GLM pixels. If none of these pixels reach the local GLM threshold, then the pulse will not be detected.

These scenarios are problematic for interpreting trends in the evolutions of LIS / GLM flashes because it is not clear to what extent the variations in pulse energy and illuminated area over time are due to the physical nature of lightning or due to detection biases. For example, both Peterson and Rudlosky (2019) and Zhang et al., (2019) noted that the energy of LIS "groups" (which approximate individual optical pulses) that comprise LIS flashes start off at a local maximum, fall to a minimum energy, and then build to a second maximum over time. LIS flashes either "start with a bang" or build up to one over time. These peaks could be due to physical lightning processes or they might be the result of LIS missing activity early in the flash. If no activity is detected before the first bright pulse from a stroke (or energetic in-cloud event in IC flashes), then it will occur at 0 ms into the flash. If this pulse occurs at the end of a LIS integration frame (or if there is channel brightening before attachment), then the bright pulse might be recorded at 2 ms into the flash. The combination of these two scenarios could lead to an initial narrow peak on the order of a few milliseconds, regardless of what CG or IC processes are involved. Alternatively, if LIS is able to detect some in-cloud activity before this initial bright pulse, then the pulse could occur at any time over the flash duration. This gives us two possible

155 explanations for the second peak at later times in LIS flashes: either that generic groups get
156 brighter over time, or that the brightest pulses cluster near the end of the flash and these
157 infrequent bright groups are driving the time-energy statistics.

158 Separating physical trends in flash evolution from trends based on what an instrument
159 can practically measure is a challenge. This is why complementary measurements from multiple
160 lightning sensors that are each sensitive to lightning phenomena that are poorly-resolved by the
161 other are a powerful tool for understanding how flashes evolve. While there have traditionally
162 been few options for multi-phenomenology analyses of global lightning from orbit, new
163 additions to existing platforms such as the Atmosphere-Space Interactions Monitor (ASIM:
164 Neubert et al., 2019) on the International Space Station (ISS) and Fly's Eye GLM Simulator
165 (FEGS: Quick et al., 2020) on the NASA ER-2 high-altitude anticraft, and new space-based
166 assets including the Space and Endo-atmospheric Nuclear detonation detection Surveillance
167 Experimentation and Risk-reduction (SENSER) payload with its Radio Frequency Sensor (RFS)
168 and Risk Reduction Optical Experiment (RROE) instruments will contribute to a growing
169 catalog of coincident lightning measurements for documenting the complete development of
170 lightning flashes in many parts of the world.

171 In this follow-up study to Peterson and Rudlosky (2019), we use the Fast On-orbit
172 Recording of Transient Events (FORTE: reviewed in Light, 2020) satellite to examine how
173 measurements of flash evolution differ between its three different instruments (including a
174 lightning imager like LIS/GLM), despite these flashes being recorded from the same Low Earth
175 Orbit (LEO) vantage point. We will focus on documenting what the high-speed optical
176 photodiode detector (PDD) and RF instrumentation can detect relative to the lightning imager
177 (termed Lightning Locating System: LLS), whose performance is expected to be similar to LIS

178 and NASA's Optical Transient Detector (OTD). Scenarios where the PDD and RF sensors detect
179 lightning activity that the LLS misses will also be discussed, as they highlight the aspects of
180 flash development that are currently not well represented by LIS / GLM but might be detected by
181 wide-FOV optical and RF space-based instrumentation.
182

183 **2 Data and Methodology**

184 The FORTE satellite was launched on August 29th, 1997 into a nearly circular orbit at
185 ~825 km altitude with an inclination of 70º and an orbital period of ~100 minutes. Unlike the
186 NASA and NOAA lightning imagers, FORTE did not perform routine clustering on the events
187 detected by its instruments – as the focus of the mission was on recording transient events, not
188 flashes. A few studies have established links between coincident RF and optical waveforms
189 (Light et al., 2001b; Suszcynsky et al., 2000, 2002; Jasobson et al., 2012), and described
190 detections at a flash level (Light et al., 2003), but a robust and comprehensive cluster feature
191 dataset like the science data from LIS or the operational data from GLM has been lacking for
192 FORTE.

193 In Peterson et al. (2021a,b), we set out to construct such a dataset that clusters the event
194 detections from all three FORTE instruments into groups, series, flashes, and thunderstorm
195 "areas" following the NASA / NOAA conventions from LIS (Christian et al,. 2000) and GLM
196 (Goodman et al., 2010). This dataset is documented at length in Peterson et al. (2021a) and the
197 components of the dataset that we will use in this study are described in the following sections.
198 See Jacobson et al. (1999) and Suszcynsky et al. (2000, 2001) for a more comprehensive
199 discussion of FORTE's capabilities, and Light (2020) for an overview of FORTE scientific

findings. Section 2.1 documents the event detections that form the basis for the larger-scale cluster features in the dataset. Section 2.2 discusses the creation of groups from LLS data and flashes from any of the three instruments, and cross-linking between the features from each instrument. Finally, Section 2.3 documents the quality controls that we use to down-select the joint cluster feature data to find cases where each reporting sensor is operating in a configuration that is a fair comparison with the LLS data.

2.1 FORTE Event Data

Lightning "events" comprising a single pixel detection during one integration frame are the basic unit of measurement in the NASA / NOAA lightning imager data. We use this concept as the basis for our event definition in the joint FORTE cluster feature data by considering the large FOV footprints of the PDD and RF system to be one "pixel" and the variable PDD and RF triggering intervals (record length plus any dead time afterwards) to be one "frame." The particularities of the events from each instrument are discussed below.

2.1.1 FORTE LLS Events

The FORTE LLS was part of the FORTE optical payload known as the Optical lightning System (OLS). The OLS operated for 12 years from late 1997 until early 2010, and provided a wealth of LLS and PDD detections of optical events from around the world. The LLS was built from a modified version of the LIS hardware with the front-end optical assembly and Charge Coupled Device (CCD) imaging array identical to LIS and the operations and signal processing module developed by Sandia National Laboratories. The primary role of LLS was to geolocate lightning sources to within its ~10 km nominal pixel footprint over its 128x128 pixel 80° square FOV that spanned a ~1200 km area below the satellite. Coincident PDD detections could then

provide high time resolution light curves for individual optical pulses. As timing was not as important for the LLS as it is for LIS / GLM due to the availability of coincident PDD observations, the LLS could afford to have a lower frame rate (405 FPS compared to 500 FPS). This provided LLS with two theoretical advantages over LIS (i.e., with all else being equal including their orbits): (1) photons detected during the additional ~0.5 ms of integration time would contribute towards overcoming the detection threshold in each pixel, making it easier to detect dim cloud pulses that persist for significant fractions of a millisecond, and (2) longer integration times mean a reduced likelihood of optical pulses being split between consecutive integration frames.

However, what the LLS reports as "events" differs from the standard NASA / NOAA definition. Raw LLS "events" are more analogous to LIS / GLM groups or series, as they contain one-or-more pixel detections that might occur in consecutive integration frames (Suszcynsky et al. 2001). Moreover, the glint filter used by LLS turned off individual pixels if illumination was detected in more than two consecutive frames. This is not the approach used by NASA to mitigate glint, and it can result in stationary persistent light sources (for example, continuing current from strokes) being missed by the LLS.

Despite these particularities of the LLS, we built our FORTE cluster feature dataset to resemble the LIS / GLM data as closely as possible. While we cannot recover missed events from the glint filter, we can convert the raw LLS "events" into features that conform to the NASA / NOAA standard by extracting the individual pixel detections and using them to create

distinct event features. From this point forward, any discussion of LLS events will describe these converted events that represent individual triggered pixels in the same integration frame.

2.1.2 FORTE PDD Events

The FORTE PDD (Kirkland et al., 2001; Suszcynsky et al., 2001) provided broadband (0.4 μm – 1.1 μm) measurements of optical lightning activity across its circular 80° FOV at a high frame rate (66,667 FPS). Unlike the LLS, which had one primary operating mode, PDD trigger settings and records lengths were reconfigured throughout the FORTE mission. The PDD could run autonomously with a noise-riding amplitude threshold trigger, or it could be triggered by either the LLS or RF system, while record lengths ranged from 1.92 ms to 6.75 ms. We are only interested in autonomous PDD triggers that have record lengths of 1.92 ms in this study. In this mode, the optical signals must exceed the average background radiance by the noise-riding threshold for a specified duration (usually 5 samples or 75 μs) to trigger the instrument. This minimum time requirement is enforced to mitigate false detections from energetic particle impacts.

The PDD also had a maximum trigger rate threshold to prevent sustained optical pulses during glint events from filling up the instrument memory. Whenever a specified number of PDD events is recorded (i.e., a multiple of 10) during a specified time interval, the PDD will turn off until the next GPS-derived 1-Hz signal. We have discussed PDD dropping out after precisely 20 triggers in both FORTE flashes that we previously analyzed in detail in Peterson et al. (2021a,b) due to this filter. It will only activate in periods with high lightning rates (including high event rates from individual flashes), and the instrument should be able to recover at the next GPS second, with only triggers in the middle of the flash being missed. However, since most

264 flashes last only a fraction of a second, this means that there are many cases of flashes that have
265 precisely 10, 20, 30, etc. PDD triggers corresponding to the specified maximum trigger count.
266 The PDD will not give a complete picture of flash evolution in these cases, and they must be
267 excluded from our analyses.

268 2.1.3 FORTE RF Events

269 The FORTE RF system (Jacobson et al., 1999; Suszcynsky et al., 2000; Shao and
270 Jacobson, 2001; Light et al., 2001b) was operational between late 1997 and 2003, and consisted
271 of three broadband VHF receivers in the 26 to 300 MHz range that were connected to two
272 identical Log-Periodic Antennas (LPAs) mounted orthogonal to each other along FORTE's 10-m
273 nadir-pointing boom. The effective FOV of the RF system was 120°, which spanned a horizontal
274 distance of ~6,000 km. The three RF receivers were divided between two RF payloads. The
275 "Two And Twenty Receiver" (TATR) payload consisted of two receivers (TATR/A and
276 TATR/B) that could each be tuned to a desired 22-MHz subband, while the remaining receiver
277 comprised the "HUndred Megahertz Receiver" (HUMR) payload that sampled a wider (85 MHz)
278 band.

279 The overall sample of RF events is heterogeneous due to differences in the trigger
280 strategy, band(s) used, record lengths, and ratios of pretrigger to posttrigger data. Of these
281 factors, the trigger strategy and record length are most critical for the present work. As with the
282 PDD, the RF system could be externally triggered by the optical instruments. To ensure
283 consistency with the reference LLS data, we only consider RF events with record lengths shorter
284 than the 2.47 ms LLS integration time that were recorded while TATR or HUMR were in their
285 autonomous trigger mode. In this autonomous mode, RF power was monitored in eight evenly-

286 spaced 1-MHz channels across the passband, and the instrument triggered whenever the power in
287 a specified number of these channels (often 5) exceeded the noise-riding background level by a
288 specified threshold (often 14-20 dB) (Jacobson et al., 1999), yielding an RF event. As HUMR
289 generally provided longer records and was commonly triggered by the PDD, almost all of the
290 event data that we consider here comes from TATR.

291 2.2 FORTE Combined-Phenomenology Cluster Feature Data

292 The FORTE cluster feature dataset (known as FORTE-CIERRA, as it shares the same
293 processing methods as the CIERRA datasets for LIS, OTD, and GLM) consists of three parallel
294 and independent data trees (one for each distinct FORTE instrument) that include all of the
295 feature levels available for LIS and GLM. This feature data is constructed following the NASA /
296 NOAA clustering techniques (Christian et al., 2000; Mach et al., 2007; Goodman et al., 2010)
297 used with LIS and GLM.

298 Contiguous events that occur in the same frame are clustered into group features that
299 describe the lightning emissions during that frame. For the PDD and RF system whose whole
300 FOV is considered one "pixel", groups are always identical to events. Groups that occur in close
301 spatio-temporal proximity are then clustered into features approximating lightning flashes.
302 Groups are determined to belong to the same flash using a Weighted Euclidean Distance (WED)
303 model with two distance terms (East-West, and North-South) and a temporal term. While the
304 temporal threshold of 330 ms is common between LIS, GLM, and the FORTE LLS, we choose
305 to use the larger 16.5 km distance threshold used for OTD and GLM for LLS clustering due to its
306 larger ~10 km pixels. However, we apply this model to group centroids, following the LIS
307 approach, rather than to group constituent events, as GLM does. For the PDD and RF system, we

neglect the distance terms in the WED model and cluster groups into flashes purely based on time differences. This is because any geospatial displacement in the PDD / RF group location data would be the result of satellite motion rather than changes in the locations of lightning below the satellite. We also use the full-fit clustering approach employed with GLM for all three FORTE instruments rather than the first-fit approach used with LIS and OTD. When a new group occurs between two existing flashes that could belong to either flash in the FORTE data, the clustering algorithm will merge the two existing flashes into a single feature.

Flash features are then used to construct series features that describe lightning activity on time scales between groups and flashes, and area features that describe thunderstorm snapshots during the FORTE overpass. Series features are defined as collections of groups originating from the same flash that are separated in time by no more than one empty frame, and describe sustained emission during a flash, for example from widespread leader development or continuing current. Finally, area features are constructed by applying the group-to-flash clustering methods to flash clusters. For LLS, we remove the temporal term and cluster areas based on geographic flash positions. For the RF system and PDD, we cluster all flashes within a time threshold approximately equal to the instrument view time. However, we do not use areas in this study, and will not focus on them here.

While the LLS cluster hierarchy is identical to its LIS / GLM counterparts, the high sample rate of the PDD and RF mean that events are no longer the bottom of their data trees. PDD / RF events are comprised of "sample" features that describe one measurement at the native sampling rate of these instruments and "pulse" features that contain multiple samples in the event record that exceed a dynamic threshold (conceptually, pulses are similar to series, but on finer

time scales). As with areas, we do not consider these sub-event features here, but they were examined in Peterson et al. (2021a,b).

Once the data trees have been constructed for each instrument, they are cross-linked between instruments by assigning "step-sibling" links to coincident features at the same level and "step-parent" links to higher-level features. For example, an LLS flash can be the step-parent of a PDD or RF event, and a LLS group within the flash might be the step-sibling of one of those PDD or RF events (since PDD / RF events are identical to groups). Thus, for every feature, we have a record of whether there was a coincident detection by another instrument and whether the coincidence was at the flash level or at the group / event level.

2.3 Identifying Acceptable-Quality Autonomous Detections in the Cluster Feature Data

Judicious quality control is important for this work because FORTE was operated in campaign mode, meaning that the configurations of its instruments were modified frequently over its mission, resulting in different types of lightning records being collected. While this flexibility provides a unique niche for FORTE research, consistency between event types is crucial for generating flash evolution statistics. Thus, we will only consider flashes where the PDD and RF configurations were LLS-like (and, by proxy, LIS-like) where each instrument was operating autonomously and producing shorter data records than the 2.47 ms integration time of the LLS. Configurations where one instrument triggered another or where the RF or PDD instruments produced long records are not considered.

We use the cross links in the cluster feature data to find all LLS flashes that are associated with PDD or RF detections with an acceptable instrument configuration. As we are comparing each instrument against the LLS, we do not require all three sensors to record each

352 flash. Flashes are considered if they trigger the LLS and the PDD or if they trigger the LLS and
353 RF system. We are also interested in flashes that occur in isolation where nearby lightning does
354 not contribute PDD or RF events during the duration of the flash. Coincident flashes would be
355 particularly troublesome if they occurred before the first LLS group or after the final group in the
356 LLS flash, as it would give the impression that the LLS is missing events, when this activity was
357 actually unrelated to the flash in question. Thus, we filter flashes that have no PDD, LLS, and RF
358 triggers >330 ms before the first group, >330 ms after the last group, or both – following the
359 temporal clustering threshold.

360 The number of LLS flashes that pass each filter are listed in Table 1. In total, 18 million
361 unique flashes were recorded by the LLS between late 1997 and early 2010. Unfortunately, many
362 of these flashes are actually artifacts from either glint or energetic particle impacts over the
363 South Atlantic Anomaly (SAA). This is a significant limitation for the LLS data record. We can
364 use the other instruments to confirm LLS flashes, but this is only possible when another
365 instrument is operating (i.e., no RF after 2003) and commanded to report events (i.e., individual
366 instruments could be turned off to limit memory use). Of the original 18 million LLS flashes,
367 only 1.2 million flashes occurred while the PDD and/or RF instruments were operating and
368 configured to trigger autonomously with record lengths < 2.47 ms. In total, 1.1 million flashes
369 were found with PDD and/or RF triggers within the flash window (duration +/- 330 ms) and
370 726,546 of these had PDD / RF events coincident with LLS groups. Imposing the isolation
371 requirement further reduces the sample size, leaving 106,336 LLS flashes that have group-level

coincidence with another instrument and that lacked any triggers before or after the flash window.

We will use this sample of LLS flashes to compare the activity recorded by the lightning imager to the other instruments. However, before examining what each type of instrument on FORTE reported from these LLS flashes, it is useful to examine how the flashes compare with measurements from the NASA lightning imagers. Table 2 lists average flash characteristics derived from OTD, LLS, and LIS data. Due to their similar orbits, the FORTE-LLS flashes are expected to most closely resemble OTD flashes, while the flashes recorded during the two LIS deployments bound the differences that can be expected from identical hardware in similar orbits. The average OTD flash consisted of 3.5 series, 4.9 groups, and 9.9 events over a 164 ms duration and 5.5 km lateral extent. The average LLS flash characteristics are close to the OTD values with 1 fewer group and event, a ~1 integration frame shorter duration, and a ~1 km larger extent (likely due to the pixel size difference). The differences between OTD and LLS flashes are mostly smaller than the differences between the LIS on the TRMM satellite and the LIS on the International Space Station (mean flash extent is the exception). For this reason, it is reasonable to expect that the differences in what LLS can see compared to the PDD or RF system are representative of what might be gained by adding FORTE-like instrumentation to the

International Space Station or flying a new satellite in a comparable orbit to these other platforms.

3 Results

The following sections will compare the evolution of LLS flashes with the temporal distributions of their constituent PDD and RF events to examine how much of the flash is detected by each of the FORTE instruments. Section 3.1 will generate overall statistics of how many detections are recorded per LLS group and compare single-sensor flash lengths. Then, Section 3.2 will examine where PDD and RF events occur relative to key points in the LLS flash (first light, brightest group, final light).

3.1 The Composition and Duration of LLS, PDD, and RF Flashes

While we previously documented the composition and duration of LIS flash features in Peterson and Rudlosky (2019), FORTE allows us to compare the pixelated lightning imager statistics with large-FOV broadband optical and RF measurements. The RF perspective on LLS flashes is expected to be quite different than what the lightning imager reports because RF is sensitive to rapid changes in electrical current while the optical instruments sense cloud illumination (which depends on current integrated over channel length and attenuated by absorption and scattering within the cloud medium).

Radiative transfer in the cloud can also lead to differences in detection between a pixelated lightning imager and a wide-FOV optical instrument like the PDD. Scattering in the cloud causes the optical emissions to be spread over a large cloud area that can exceed 10,000

410 km^2 in some cases (Peterson et al., 2017). All of the photons that escape to space and are directed
411 towards the satellite count towards exceeding the threshold of a PDD-like instrument, regardless
412 of the path they took to the satellite. However, a pixelated instrument like the LLS requires the
413 local threshold in each pixel to be exceeded for an event to be declared. Thus, faint illumination
414 far from the optical emitter often goes undetected by a lighting imager, and pulses can escape
415 detection entirely if their optical emissions are distributed too broadly throughout the cloud. The
416 pulse may have been energetic enough to trigger the PDD, but if no single 10-km pixel exceeds
417 the detection threshold, the LLS will not trigger.

418 These factors will affect the relative trigger rates between the three instruments. Figure 1
419 shows two-dimensional histograms comparing the number of (a) LLS, (b) PDD, and (c) RF
420 events to the number of LLS groups in each flash, and also histograms for the number of LLS
421 (d), PDD (e), and RF (F) events per LLS group. Only flashes that are isolated in time where the
422 RF and PDD configurations are LLS-like and not subject to the PDD maximum trigger count (as
423 described in Section 2) are considered.

424 The comparisons between the LLS features in Figure 1a,d show that LLS groups
425 typically consist of events in 2-3 contiguous pixels on the CCD imaging array. Around 8% of
426 flashes consist of only single-event groups, ~40% of flashes have 2 events for each of its groups,
427 ~88% of flashes have < 5 events per group and only the top ~2% of flashes have more than 10
428 events per group. In these latter cases, multi-event groups far outnumber single-pixel detections
429 – ether due to frequent bright pulses (as with high group counts in Figure 1a) or due to high

thresholds or backgrounds preventing faint emissions from being detected (as with low group counts in Figure 1a, where the flash may be comprised of a single 50-event group).

We perform the same analyses for PDD events in Figure 1b,e. Note that horizontal depressions exist at multiples of 10 triggers. These correspond to flashes that reached the maximum PDD trigger rate, and are excluded here. Values are not zero due to the removal of PDD artifact events in otherwise valid flashes. For example, a flash with 11 PDD events might have an energetic particle impact in one of its waveforms, and the removal of this event would cause the flash to be reported as a 10-event flash.

As they are both optical instruments, the numbers of PDD events and LLS groups are correlated. However, there is also considerable spread in the data on both sides of the 1:1 line (solid line in Figure 1a-c). A flash with 10 LLS groups might only trigger the PDD once, or it could have as many as 38 distinct PDD events. Despite this range, flashes typically have 1-2 PDD events per LLS group with ~18% of flashes containing more LLS groups than PDD events, ~20% having an equal number of triggers by both instruments, and the remaining ~62% having more PDD events than LLS groups. Differences between the LLS and PDD trigger rates in the same sample of flashes are due to multiple factors including thresholding differences and signal characteristics – such as the optical pulse width (the PDD requires above-amplitude signals for at least 75 μs), spectral content (the LLS is a narrow-band instrument at 777.4 nm), spatial broadening from scattering in the cloud medium (the LLS is a pixelated sensor), and record length (the 1.92 ms for the PDD compared to 2.47 ms for the LLS). This all means that while the PDD generally sees more flash activity than the LLS, the relative sensitivity of the two

optical instruments depends on the situation. There are also some flashes that the LLS is able to resolve with greater detail than the PDD.

The RF picture of these flashes, meanwhile, differs considerably from the optical LLS perspective. As with the PDD, the RF instrumentation can resolve activity missed by the LLS (and vice versa), but there is no real correlation between the number of RF events and LLS groups in Figure 1c. A single-group flash may have up to 20 RF events, while a 44-group flash might just trigger the RF system once. Still, the RF system typically provides at least as many unique triggers for a given flash as the LLS. Around 31% of flashes have more LLS groups than RF events, another 22% have the same number of RF events and LLS groups, while nearly half of all flashes (47%) have more RF triggers than LLS groups.

These trigger rate differences between the three FORTE instruments affect how flashes appear to evolve from orbit. Assessing how flashes change from first light through the end of the flash is complicated by the fact that there is often not a common reference window. A LIS / LLS flash will always have a first group, but that first group could result from in-cloud activity early in the flash, or it could correspond to a return stroke tens of milliseconds into the flash with all previous activity being too faint to resolve. Comparing the durations of a common set of flashes that are apparent to the LLS, PDD, and RF system on FORTE is a good example of this. Figure 2 shows (a) histograms of flash durations computed from only the events recorded by each instrument and (b) histograms of differences in flash duration between each instrument. Of the three instruments, RF flashes are most likely to consist of a single event (36%), causing an apparent duration of 0 ms, while PDD flashes are least likely to contain just one event (14%). However, longer-lasting RF and PDD flashes both tend to be at least slightly longer than their LLS counterparts. While 32% of LLS flashes are longer than RF flashes (including the single RF

474 event cases), 37% of RF flashes are longer than their corresponding LLS flashes, and the
475 remaining 31% are have the same duration. At the same time, 14% of PDD flashes are shorter
476 than their LLS counterpart, 25% are the same length, and the remaining 61% are longer-lasting
477 than the coincident LLS flash. This means that the RF system and especially the PDD are not just
478 able to see certain flashes in more detail, they are detecting periods of the flash evolution that are
479 outside of the LLS flash window. This activity could be before the first LLS group or after the
480 final LLS group. Either way, this missed activity affects the statistics of how flashes develop
481 over time presented in Peterson and Rudlosky (2018) and Zhang et al., (2020).

482

483 3.2 Timing of Optical and RF Events in Isolated LLS Flashes

484 The FORTE PDD and RF system can detect activity that is missed by its lightning
485 imager. In this section, we explore where this activity occurs in the flash and how it impacts
486 measurements of flash evolution. Figure 3 examines how often the first PDD or RF event occurs
487 before, coincident with, and after the first LLS group. Two-dimensional histograms are presented
488 in (a) for the PDD and (c) for the RF system between the time delay from LLS first light and the
489 number of LLS groups in the flash. Figure 3b and c, then, show single cumulative distributions
490 for flashes within the 0-20 LLS group range shown in Figure 3a and d (black) , and flashes with
491 > 20 groups (blue).

492 Note that because we are only considering flashes that are isolated in time, flashes with
493 LLS, PDD, or RF events >330 ms (the clustering time threshold) before the start of the flash are
494 not included. The histograms begin at the vertical line at -330 ms because these events – if
495 detected by the LLS – would be clustered into the same flash. Flashes that are poorly resolved by

the LLS to the point where the first >330 ms of activity in the flash is either not detected at all by the LLS or is intermittently detected (i.e., causing the flash to be split into multiple LLS features) are not considered in these statistics. While these flashes contribute to LLS performance in resolving flash evolution, they cannot be reliably distinguished from high flash rate environments where the whole-FOV PDD and RF detections might be assigned to the wrong flash.

The cumulative distribution functions (CDFs) in Figure 3 can be divided into three sections: a long plateau where the first PDD / RF triggers occur well ahead of the first LLS group, a narrow peak around 0 ms where the PDD / RF triggers occur at around the same time as the first LLS group, and a second smaller plateau where the first PDD / RF triggers occur well after the first LLS group. The boundaries of these regions are somewhat subjective and vary between instruments and by LLS group count, which can be a proxy for how well the flash is resolved by the LLS. LLS flashes that consist of just 1-2 groups are probably not well resolved with only the single brightest pulse (for example, the first return stroke in CG flashes) being detected. Such cases stand to benefit the most from coincident PDD or RF measurements that resolve activity before the initial LLS detection – and, indeed, the CDFs near the bottom of the plot in Figure 3a are shifted to the left to have a longer plateau before first LLS light. Flashes that are better resolved by the LLS (containing more groups over the flash duration) are less likely to have notable activity before the start of the LLS flash, as we see with the rightward drift in the CDFs with increasing group count in Figure 1a.

A threshold of 10 ms should be sufficient to identify flashes whose first PDD / RF emissions are significantly offset from the first LLS group. This would correspond to 4 LLS integration frames, which would ensure that the optical illumination captured by LLS results

519 from a different process than what first triggered the PDD or RF system. In total, 41% (44%) of
520 1-20 group LLS flashes are preceded by PDD (RF) activity at least 10 ms before the first LLS
521 group, 51% (31%) have the first PDD (RF) trigger within 10 ms of the first LLS group –
522 including 40% (20%) where the first events were simultaneous – and the remaining 8% (25%)
523 have the first PDD (RF) event after the first LLS group.

524 Thomas et al. (1999) found that lightning imagers (in this case LIS) tended to trigger late
525 in the discharge compared to an LMA and attributed these differences to source altitude (LIS
526 preferentially detected sources above 7-10 km altitude), extensive illumination over large
527 portions of the lightning "tree" in IC flashes, and late-stage components and subsequent strokes
528 in CG flashes. Our FORTE PDD results suggest that these delays are at least partially due to the
529 design of the lightning imager and background noise constraints imposed by the space-based
530 vantage point, rather than solely from detection issues inherent in the optical phenomenology. In
531 the 41% of 0-20 group flashes where the early optical emissions trigger the PDD while failing to
532 trigger the LLS, the median time delay between the PDD and LLS is 121 ms. Even within the
533 same phenomenology, the lightning imager is still often delayed relative to a wide-FOV
534 instrument with the same vantage point. Lightning imagers like LLS, LIS, or GLM would be
535 expected to capture this activity if they could be made more sensitive by either lowering the
536 trigger threshold or either increasing the pixel size or summing over pixels so more of the pulse
537 contributes to overcoming the threshold.

538 Meanwhile, the RF system on FORTE operates in the VHF band like the LMA used by
539 Thomas et al. (1999) and might be considered a space-based analog to a ground-based LMA
540 receiver. Delays between the first LLS group and first RF event capture not only differences in
541 sensitivity, but also phenomenological differences between optical and RF detection. In the 44%

of 0-20 group flashes with RF events > 10 ms from first LLS light, the median LLS delay relative to RF is 142 ms. The median LLS delay relative to RF being on a similar scale to the LLS delay relative to the PDD suggests that the pixelated nature of the LLS is inhibiting detection more than phenomenological differences. Instead, the phenomenology of the wide-FOV sensor has a greater impact on the proportions of flashes that trigger before, around the same time as, or after first LLS light. When the LLS first triggers, the PDD will usually have or have had its first event. With RF, the probabilities of the first event occurring before, during, or after the first LLS group are more even, by comparison, because the optical and RF detections are independent from one another and sensitive to different aspects of the flash. Certain LLS flashes - like the hybrid CG case we analyzed in Peterson et al. (2021b) - start with strong VHF TIPP well ahead of first optical light, but this is not the case for all flashes.

We apply the same analyses to the final LLS group in each flash in Figure 4. The trends in these distributions are largely inverted compared to the first LLS group analyses in Figure 3. Fewer of the final PDD triggers occur before the last LLS group than afterwards. Flashes that are poorly-resolved by the LLS and consist of just 1-2 groups are the most likely to have PDD triggers following the final LLS group, as the PDD detects activity that is missed by the LLS. Flashes with 20+ LLS groups, meanwhile, commonly have the final PDD trigger occur before the final LLS group. The RF trends also mirror the PDD, but with a greater fraction of final RF events before the final LLS group and fewer RF events coincident with the final LLS group. When there are PDD (RF) events following the final LLS group, the PDD (RF system) reports a median of 109 ms (142 ms) of activity after LLS stops triggering.

Figures 3 and 4 categorize flashes by group count to comment on poorly-resolved LLS flashes that might only consist of 1-2 groups. In the following analyses, we will, instead, shift

565 our focus to LLS flash duration. Categorizing flashes by duration makes it possible to show the
566 full flash length in a single plot (diagonal lines in panels a and c). The timing of the most
567 energetic PDD events and most powerful RF events in each LLS flash is documented in Figure 6
568 relative to the brightest LLS group and Figure 7 relative to the first LLS group.

569 The first question that we address is how often the brightest PDD / RF events correspond
570 to the brightest LLS group. For the PDD, 21% of the brightest events per flash occur before the
571 top LLS group, 61% occur at the same time, and the remaining 18% occur later. The most
572 energetic PDD events may not correspond to the most energetic LLS group if the energy is
573 spread over time (such that the length difference between the 1.92 ms PDD records and 2.47 ms
574 LLS integration time becomes important) or horizontally across the cloud medium (LLS pixels
575 that do not contain enough energy to exceed the detection threshold will not be counted), or if the
576 signal has less energy concentrated in the 777.4 nm spectral band than what is typical for
577 lightning emissions. The frequency of matches between the top PDD and LLS detections
578 depends on flash duration, where short-lived flashes are most likely to have PDD/LLS agreement
579 and long-lasting flashes (including cases > 500 ms in duration) are more likely to have their most
580 energetic PDD events offset from the top LLS group. These long-lasting flashes are expected to
581 have extensive lateral development, where emissions from broad optical sources may be divided
582 between multiple LLS pixels. While the PDD would capture all of the energy from these sources,
583 individual LLS pixels may not trigger if they are too dim, causing some of the optical energy
584 form the pulse to be lost.

585 Coincidence between the brightest LLS group and most powerful RF event is less
586 common than LLS/PDD coincidence. 37% of the top RF events occur before the brightest LLS
587 group, 32% are coincident with the top LLS group, and the remaining 31% occur following the

588 top LLS group. As with the PDD, looking only at flashes > 500 ms in duration reduces the
589 frequency that the top LLS group matches the top RF event. The top RF emissions come from
590 events that are not particularly energetic in terms of LLS energy. This includes a sizable fraction
591 of Narrow Bipolar Events (NBEs) (Light and Jacobson, 2004) as well as strokes and other
592 optically-bright processes that are not fully captured by the pixelated lightning imager due to
593 attenuation by the clouds.

594 The final flash evolution analyses shown in Figure 6 describe the timing of the top
595 PDD/RF events relative to the start of the LLS flash. These plots provide an expanded view of
596 the top optical and RF events compared to our previous analyses (Figure 5 in Peterson and
597 Rudlosky, 2019). We also add additional curves to the cumulative histograms in Figure 6b and d
598 to account for flashes of intermediate durations within the 0-500 ms range.

599 The behavior of these particularly-bright optical events is important because these pulses
600 have a disproportionate impact on the average group area / energy trends presented in Zhang et
601 al. (2020). Increasing average group areas at certain points in time could result from a general
602 increase in the area of all groups in response to physical changes to the flash, or it could be due
603 to an anomalous concentration of particularly-bright groups from high-energy phenomena (like
604 strokes or K-changes) at these points in the flash evolution. Our prior work suggests that the
605 latter possibility is more likely. Typical LIS / LLS flashes are comprised of mostly small / dim
606 groups offset by a very small number of exceptionally-bright groups (i.e., Figure 4a in Peterson
607 and Rudlosky, 2019). Peterson and Rudlosky (2019) reported the frequency of these bright LIS
608 groups over the flash duration using a normalized energy that scaled with the typical energy of
609 the myriad dim groups in the flash. The frequencies of bright groups at all three energy
610 thresholds considered ($1\boldsymbol{\sigma}$, $2\boldsymbol{\sigma}$, or $3\boldsymbol{\sigma}$) had a sharp initial peak at first light, then a minimum

followed by a second broad peak towards the end of the flash – matching the behavior of the group area / energy curves for IC flashes shown in Figures 5 and 6 of Zhang et al. (2020).

The PDD distributions also agree with this assessment. The brightest optical pulses in Figure 6b occur most frequently alongside the first LLS group (42% of all 0-500 ms flashes) compared to any other specific point in the flash. Another 51% of top PDD events in these flashes occur following the first LLS group, and then the remaining 7% of events occur before the start of the LLS flash. As LLS flash durations increase, fewer top PDD events are noted at or before the first LLS group. Thus, the initial peak at 0 ms is eroded, while more of the top PDD events occur during or after the LLS flash.

The individual curves for flashes of each duration additionally show a pronounced peak at the end of the flash. These peaks come from cases where the brightest optical emissions occur alongside the final LLS group. The prominence of this peak depends on the width of bin used to categorize flash duration. If we only selected flashes that were precisely 100 ms in duration, the peak would be instantaneous. If we use bins with a finite size, however, then the final group in each flash within that bin will be spread out over the bin width. For larger bins, like the 0-500 ms curve in Figure 6b, the later peak is completely obscured. We use an intermediate bin size of 20 ms for the curves in Figure 6b that correspond to each 100-ms interval aligned to the stated duration. Thus, the 100 ms curve includes flashes between 100 ms and 120 ms. This behavior is not evident in the average group aera / energy curves in Figure 7 of Zhang et al. (2020), probably due to the 100 ms window (or 500 ms for the final window) that they used. This final peak could be due to a physical lightning process that prevents subsequent pulses – perhaps by exhausting the remaining charge that can be accessed by the flash, or cutting parts of the

633 flash off so later pulses become too faint to be detected (i.e,. near the cloud-top, as we saw
634 following the return stroke in Peterson et al., 2021b).

635 The most powerful RF events in Figure 6c-d show similar behavior to the top PDD
636 events, despite the different phenomenology and reduced RF sample size compared to the
637 PDD. The key difference is that the top RF event occurs more frequently before the first LLS
638 group. This occurs in 25% of all 0-500 ms LLS flashes (compared to 7% for the PDD), and
639 in 11% of 500+ ms flashes (compared to 3% for the PDD). The reason for this is the
640 previously-noted prevalence of phenomena that are optically dark in the bands sampled by
641 the LLS and PDD early in the flash – the most notable example is the case of TIPPs from
642 NBEs that are some of the most powerful natural RF emitters in the VHF band (Light and
643 Jacobson, 2002; Jacobson et al., 2012). Note that NBEs at the beginning of normal lightning
644 flashes do not represent all NBEs. Many occur in isolation or in pairs not associated with
645 typical flashes (Nag et al., 2010). Moreover, these events also include other processes
646 (including strokes) that might not result in a LLS trigger.

647 These results demonstrate the value of having coincident space-based lightning
648 measurements to assess flash evolution. Different sensors (even with the same underlying
649 phenomenology like the LLS and PDD) provide additional insights into how flashes evolve
650 that might be missed by another instrument. These missed portions of the flash are
651 important for informing the physics of the discharge and its potential impacts on the
652 broader Earth system. Current and future missions that provide comprehensive
653 measurements of global lightning from the same spacecraft or that add new instruments /

654 phenomenologies to existing orbital lightning measurements are well-situated to generate
655 new insights into how flashes evolve.

656

657 **4 Conclusion**

658 In this study, we examine the events reported by the three instruments on the FORTE
659 satellite to compare the performance of the whole-FOV optical and RF instrumentation relative
660 the pixelated lightning imager, and how these differences affect measurements of flash evolution
661 taken from the same space-based vantage point. The lightning imager will generally trigger once
662 the total optical energy of the pulse reaches the particular threshold for detection, but this is not
663 always the case. Certain optical pulses may be detected by the PDD but missed by the LLS. We
664 suggest that this is due to differences in instrument sensitivity and the pixelated nature of the
665 LLS that requires the total energy in each individual pixel to exceed the detection threshold.
666 While localized sources with high energy densities are resolved by both instruments, pulses that
667 have been spatially broadened by scattering in the cloud medium (including quick pulses from
668 strokes) and faint pulses from horizontally-extensive sources may produce enough light to trigger
669 the PDD while lacking the necessary energy density to trigger the LLS.

670 The PDD and RF system are also shown to better capture certain aspects of flash
671 development that are missed by the LLS. This is consistent with previous comparisons with
672 lightning imagers showing that they tend to trigger late in the discharge. Even though the LLS
673 and PDD are both optical instruments, the PDD routinely detects pulses before the first LLS
674 event and after the end of the LLS flash. The RF system detects even more activity outside of the
675 LLS flash duration. This activity missed by the LLS is likely the origin of previous findings that

676 energetic optical pulses are typically found either at the very beginning of the flash or near the
677 end of the flash. Bright pulses from processes such as strokes may occur throughout the flash
678 duration, but if the instrument misses the early (or late) portions of the flash (either due to a high
679 threshold or low energy density), then the stroke might be the first (or last) optical pulse detected
680 by the instrument. There will always be a first pulse in the LLS flash, but that pulse may not be
681 the true beginning of the flash. If in-cloud activity is detected before the stroke or other bright
682 process, then the brightest pulse in the flash will occur later towards the end of the flash after it
683 grows to an appreciable size.

684 The additional information provided by instruments like the FORTE PDD and RF system
685 are useful on their own, but joint analysis with a lightning imager is particularly powerful for
686 providing a comprehensive view of flash evolution. Lightning emissions have a variety of pulse
687 widths, powers, and energies in the optical and RF portions of the electromagnetic spectrum. A
688 diverse collection of instrumentation is key for recording every aspect of how flashes develop
689 over time. Gaining this perspective for global lightning will require multi-sensor measurements
690 from space-based platforms. While FORTE was a pioneer in this effort, current and future
691 missions will further advance our understanding on lightning physics worldwide.

692

693 **Acknowledgments**

694 Los Alamos National Laboratory is operated by Triad National Security, LLC, under contract
695 number 89233218CNA000001. Research presented in this article was supported by the
696 Laboratory Directed Research and Development program of Los Alamos National Laboratory

under project number 20200529ECR.The data presented in this study are located at Peterson (2022).

References

Bitzer, P. M., 2017: Global distribution and properties of continuing current in lightning, *J. Geophys. Res. Atmos.*, **122**, 1033–1041, doi:10.1002/2016JD025532

Bitzer, P.M. and H.J. Christian, 2015: Timing Uncertainty of the Lightning Imaging Sensor. *J. Atmos. Oceanic Technol.*, **32**, 453–460, https://doi.org/10.1175/JTECH-D-13-00177.1

Boggs, L. D., N. Liu, M. Peterson, S. Lazarus, M. Splitt, F. Lucena, A. Nag, and H. Rassoul, 2019: First observations of gigantic jets from geostationary orbit. *Geophys. Res. Lett.*, **46**. https://doi.org/10.1029/2019GL082278

Budden, K. G., 1985: The Propagation of Radio Waves. *Cambridge Univ. Press*, New York

Cecil, D. J., D. E. Buechler, and R. J. Blakeslee, 2014: Gridded lightning climatology from TRMM-LIS and OTD: Dataset description. *Atmos. Res.,* **1350136,** 404-414

Christian, H. J., R. J. Blakeslee, S. J. Goodman, and D. M. Mach (Eds.), 2000: Algorithm Theoretical Basis Document (ATBD) for the Lightning Imaging Sensor (LIS), NASA/Marshall Space Flight Center, Alabama. (Available as http://eospso.gsfc.nasa.gov/atbd/listables.html, posted 1 Feb. 2000)

Christian, H. J., R. J. Blakeslee, D. J. Boccippio, W. L. Boeck, D. E. Buechler, K. T. Driscoll, S. J. Goodman, J. M. Hall, W. J. Koshak, D. M. Mach, and M. F. Stewart, 2003: Global frequency and distribution of lightning as observed from space by the Optical Transient Detector. *J. Geophys. Res.*, **108**(D1), ACL-4.

718 Cummins, K. L., M. J. Murphy, E. A. Bardo, W. L. Hiscox, R. B. Pyle, and A. E. Pifer, 1998: A
719 combined TOA/MDF technology upgrade of the U.S. National Lightning Detection
720 Network. *J. Geophys. Res.*, **103**, 9035–9044
721 Cummins, K.L., and M. J. Murphy, 2009: An Overview of Lightning Locating Systems: History,
722 Techniques, and Data Uses, With an In-Depth Look at the U.S. NLDN, *IEEE Tramn. on*
723 *Electromag. Compat.*, **51**, 3, pp. 499-518, doi: 10.1109/TEMC.2009.2023450.
724 Eack, K. B. (2004), Electrical characteristics of narrow bipolar events, *Geophys. Res. Lett.*, **31**,
725 L20102, doi:10.1029/2004GL021117.
726 Goodman, S. J., D. Mach, W. J. Koshak, and R. J. Blakeslee, 2010: GLM Lightning Cluster-
727 Filter Algorithm (LCFA) Algorithm Theoretical Basis Document (ATBD). NOAA
728 NESDIS Center for Satellite Applications and Research. (Available as https://www.goes-
729 r.gov/products/ATBDs/baseline/Lightning_v2.0_no_color.pdf, posted 24 Sept. 2010)
730 Goodman, S. J., R. J. Blakeslee, W. J. Koshak, D. Mach, J. Bailey, D. Buechler, L. Carey, C.
731 Schultz, M. Bateman, E. McCaul Jr., and G. Stano, 2013: The GOES-R geostationary
732 lightning mapper (GLM). *J. Atmos. Res.,* **125-126**, 34-49
733 Holden, D. N., C. P. Munson, and J. C. Devenport, 1995: Satellite observations of
734 transionospheric pulse pairs, Geophys. Res. Lett., **22**, 889–892
735 Jacobson, A. R., S. O. Knox, R., Franz, and D. C. Enemark, 1999: FORTE observations of
736 lightning radio-frequency signatures: Capabilities and basic results. *Radio Sci.*, **34** (2),
737 337– 354, doi:10.1029/1998RS900043
738 Jacobson, A. R., K. L. Cummins, M. Carter, P. Klingner, D. Roussel-Dupré, and S. O. Knox,
739 2000: FORTE radio-frequency observations of lightning strokes detected by the National

Lightning Detection Network. *J. Geophys. Res.*, **105** (D12), 15653– 15662, doi:10.1029/2000JD900103

Jacobson, A. R., and X.-M. Shao, 2002: FORTE satellite observations of very narrow radiofrequency pulses associated with the initiation of negative cloud-to-ground lightning strokes. *J. Geophys. Res.*, **107** (D22), 4661, doi:10.1029/2001JD001542

Jacobson, A. R., T. E. L. and Light, 2003: Bimodal radio frequency pulse distribution of intracloud-lightning signals recorded by the FORTE satellite. *J. Geophys. Res.*, **108**, 4266, doi:10.1029/2002JD002613, D9

Jacobson, A. R., & Light, T. E. L. (2012, February). Revisiting" Narrow Bipolar Event" intracloud lightning using the FORTE satellite. In *Annales geophysicae* (Vol. 30, No. 2, pp. 389-404). Copernicus GmbH.

Jacobson, A. R., Light, T. E. L., Hamlin, T., & Nemzek, R. (2013). Joint radio and optical observations of the most radio-powerful intracloud lightning discharges. *Annales Geophysicae (09927689)*, *31*(3).JPL, 2019: Global Ionospheric Maps. Accessed 7 May 2019, https://iono.jpl.nasa.gov/gim.html

Koshak, W. J., 2010: Optical characteristics of OTD flashes and the implications for flash-type discrimination. *J. Atmos. Oceanic. Technol.,* **27,** 1,822 – 1,838

Koshak, W. J., & Solakiewicz, R. J. (2015). A Method for Retrieving the Ground Flash Fraction and Flash Type from Satellite Lightning Mapper Observations, *Journal of Atmospheric and Oceanic Technology*, *32*(1), 79-96. Retrieved Feb 4, 2021, from https://journals.ametsoc.org/view/journals/atot/32/1/jtech-d-14-00085_1.xml

Le Vine, D. M. (1980). Sources of the strongest RF radiation from lightning. *Journal of Geophysical Research: Oceans*, *85*(C7), 4091-4095.

763 Light, T. E., D. M. Suszcynsky, and A. R. Jacobson, 2001a: Coincident radio frequency and
764 optical emissions from lightning, observed with the FORTE satellite. *J. Geophys. Res.*,
765 **106** (D22), 28223– 28231, doi:10.1029/2001JD000727
766 Light, T. E., D. M. Suszcynsky, M. W. Kirkland, and A. R. Jacobson, 2001b: Simulations of
767 lightning optical waveforms as seen through clouds by satellites. *J. Geophys. Res.*, **106**
768 (D15), 17103– 17114, doi:10.1029/2001JD900051
769 Light, T. E. L., and A. R. Jacobson, 2002: Characteristics of impulsive VHF lightning signals
770 observed by the FORTE satellite. *J. Geophys. Res.*, **107** (D24), 4756,
771 doi:10.1029/2001JD001585
772 Lojou, J.-Y., K. L. Cummins, 2004: On the representation of two- and three-dimensional total
773 lightning information. In Preprints, Conference on Meteorological Applications of
774 Lightning Data (pp. Paper 2.4, AMS Annual Meeting, San Diego, CA, USA)
775 Mach, D. M., H. J. Christian, R. J. Blakeslee, D. J. Boccippio, S. J. Goodman, and W. L. Boeck,
776 2007: Performance assessment of the Optical Transient Detector and Lightning Imaging
777 Sensor. *J. Geophys. Res., **112***, D09210
778 Massey, S. R., S. O. Knox, R. C. Franz, D. N. Holden, and C. T. Rhodes, 1998: Measurements of
779 transionospheric radio propagation parameters using the FORTE satellite. *Radio Sci.*, **33**,
780 1739–1753
781 Mazur, V., P. R. Krehbiel, and X.-M. and Shao, 1995: Correlated high-speed video and radio
782 interferometric observations of a cloud-to-ground lightning flash. *J. Geophys. Res.*, **100**
783 (D12), 25731– 25753, doi:10.1029/95JD02364

784 Mazur, V., X.-M. Shao, and P. R. Krehbiel, 1998: "Spider" lightning in intracloud and positive
785 cloud-to-ground flashes. *J. Geophys. Res.*, **103** (D16), 19811– 19822,
786 doi:10.1029/98JD02003
787 Nag, A., V. A. Rakov, D. Tsalikis, and J. A. Cramer, 2010: On phenomenology of compact
788 intracloud lightning discharges. *J. Geophys. Res.*, **115**, D14115,
789 doi:10.1029/2009JD012957
790 Peterson, M., 2019a: Research applications for the Geostationary Lightning Mapper operational
791 lightning flash data product. *J. Geophys. Res.*, **124**, 10205– 10231.
792 https://doi.org/10.1029/2019JD031054
793 Peterson, M., 2019b: Using lightning flashes to image thunderclouds. *J. Geophys. Res.*, **124**,
794 10175– 10185. https://doi.org/10.1029/2019JD031055
795 Peterson, M., 2020: Modeling the transmission of optical lightning signals through complex 3-D
796 cloud scenes. *Journal of Geophysical Research: Atmospheres*, **125**, e2020JD033231.
797 https://doi.org/10.1029/2020JD033231
798 Peterson, M., 2022: FORTE Event Time-in-Flash Database,
799 https://doi.org/10.7910/DVN/OJODZ7, Harvard Dataverse, DRAFT VERSION
800 Peterson, M. J. and C. Liu, 2011: Global statistics of lightning in anvil and stratiform regions
801 over the tropics and subtropics observed by TRMM, *J. Geophys. Res.*, **116**, D23, doi:
802 10.1029/2011JD015908
803 Peterson, M. J. and C. Liu, 2013: Characteristics of lightning flashes with exceptional
804 illuminated areas, durations, and optical powers and surrounding storm properties in the
805 tropics and inner subtropics, *J. Geophys. Res.*, **118**, 11,727-11,740, doi:
806 10.1002/jgrd.50715

807 Peterson, M. J., W. Deierling, C. Liu, D. Mach, C. Kalb, 2017a: The properties of optical
808 lightning flashes and the clouds they illuminate. *J. Geophys. Res. Atmos*., **122**, 423–442,
809 doi:10.1002/2016JD025312
810 Peterson, M. J., S. Rudlosky, and W. Deierling, 2017b: The evolution and structure of extreme
811 optical lightning flashes. *J. Geophys. Res. Atmos*., **122**, doi: 10.1002/2017JD026855
812 Peterson, M., S. Rudlosky, and W. Deierling, 2018: Mapping the Lateral Development of
813 Lightning Flashes from Orbit. *J. Geophys. Res. Atmos.*, **123**, 9674– 9687.
814 https://doi.org/10.1029/2018JD028583
815 Peterson, M., S. Rudlosky, 2019: The time evolution of optical lightning flashes. *J. Gephys. Res.,*
816 **124**, 333– 349. https://doi.org/10.1029/2018JD028741
817 Peterson, M. J., Lang, T. J., Bruning, E. C., Albrecht, R., Blakeslee, R. J., Lyons, W. A., et al.,
818 2020a: New World Meteorological Organization certified megaflash lightning extremes
819 for flash distance (709 km) and duration (16.73 s) recorded from space. *Geophys. Res.*
820 *Lett.*, **47**, e2020GL088888. https://doi.org/10.1029/2020GL088888
821 Peterson, M., S. Rudlosky, and D. Zhang, 2020b: Thunderstorm Cloud-Type Classification from
822 Space-Based Lightning Imagers. *Mon. Wea. Rev.*, **148**, 1891–1898,
823 https://doi.org/10.1175/MWR-D-19-0365.1.
824 Peterson, M., and G. Stano, 2021: The Hazards Posed by Mesoscale Lightning Megaflashes.
825 *Earth Interactions*, *25*(1), 46-56. Retrieved Aug 7, 2021, from
826 https://journals.ametsoc.org/view/journals/eint/25/1/EI-D-20-0016.1.xml
827 Peterson, M., Light, T. E. L., & Shao, X.-M. (2021a). Combined optical and radio-frequency
828 measurements of a lightning megaflash by the FORTE satellite. *Journal of Geophysical*
829 *Research: Atmospheres*, 126, e2020JD034411. https://doi.org/10.1029/2020JD034411

Peterson, M., Light, T. E. L., & Shao, X.-M. (2021b). Combined optical and radio-frequency perspectives on a hybrid Cloud-to-Ground lightning flash observed by the FORTE satellite. *Journal of Geophysical Research: Atmospheres*, 126, e2020JD034152. https://doi.org/10.1029/2020JD034152

Rison, W., R.J. Thomas, P.R. Krehbiel, T. Hamlin, and J. Harlin, 1999: A GPS-based three-dimensional lightning mapping system: initial observations in central New Mexico. *Geophys. Res. Lett*., **26**, 23, 3573-3576.

Rison, W., P. R. Krehbiel, M. G. Stock, H. E. Edens, X. M. Shao, R. J. Thomas, M. A. Stanley, and Y. Zhang, 2016: Observations of narrow bipolar events reveal how lightning is initiated in thunderstorms. *Nature communications*, *7*(1), 1-12. DOI: https://doi.org/10.1038/ncomms10721.

Shao, X.-M., 2018: Broadband RF Interferometric Mapping and Polarization (BIMAP) observations of Mini-Discharges in thunderstorms. AGU Fall Meeting 2018, Washington, DC, Amer. Geophys. Union. https://agu.confex.com/agu/fm18/meetingapp.cgi/Paper/422277

Shao, X.-M., and A. R. Jacobson, 2001: Polarization observations of broadband VHF signals by the FORTE satellite. *Radio Sci.*, **36** (6), 1573– 1589, doi:10.1029/2000RS002600

Shao, X.-M., and A. R. Jacobson, 2002: Polarization observations of lightning-produced VHF emissions by the FORTE satellite, *J. Geophys. Res*., **107** (D20), 4430, doi:10.1029/2001JD001018

Smith, D. A., X.-M. Shao, D. N. Holden, C. T. Rhodes, M. Brook, P. R. Krehbiel, M. Stanley, W. Rison, and R. J. Thomas, 1999: A distinct class of isolated intracloud lightning

852 discharges and their associated radio emissions. *J. Geophys. Res.,* **104** (D4), 4189– 4212,
853 doi:10.1029/1998JD200045
854 Soler, S., Pérez-Invernón, F. J., Gordillo-Vázquez, F. J., Luque, A., D., Li, Malagón-Romero, A.,
855 et al. (2020). Blue optical observations of narrow bipolar events by ASIM suggest corona
856 streamer activity in thunderstorms. *Journal of Geophysical Research: Atmospheres*, 125,
857 e2020JD032708. https://doi.org/10.1029/2020JD032708
858 Suszcynsky, D. M., M. W. Kirkland, A. R., Jacobson, R. C. Franz, S. O. Knox, J. L. L. Guillen,
859 and J. L. Green, 2000: FORTE observations of simultaneous VHF and optical emissions
860 from lightning: Basic phenomenology. *J. Geophys. Res.*, **105** (D2), 2191– 2201,
861 doi:10.1029/1999JD900993
862 Suszcynsky, D. M., T. E. Light, S., Davis, J. L., Green, J. L. L. Guillen, and W. Myre, 2001:
863 Coordinated observations of optical lightning from space using the FORTE photodiode
864 detector and CCD imager. *J. Geophys. Res.*, **106** (D16), 17897– 17906,
865 doi:10.1029/2001JD900199
866

867 **Table 1.** LLS flash counts that meet quality filters based on isolation from other flashes and
868 coincidence with the other FORTE sensors
869

	All LLS Flashes	LLS Flashes with Desirable PDD and/or RF Configuration	LLS Flashes with Desirable Configuration and PDD or RF Coincidence:	
			In Flash	In Group
No Isolation Requirement	18,009,006	1,245,192	1,111,496	726,546
Isolated Before Flash	1,895,931	230,984	182,994	153,294
Isolated After Flash	1,876,707	229,292	183,068	153,706
Isolated Before and After	1,222,858	152,131	118,354	106,336

870
871
872 **Table 2.** Comparisons between flash characteristics measured by the FORTE-LLS and NASA's
873 OTD and LIS instruments
874

Flash Parameter	OTD	FORTE-LLS	|Difference|	TRMM-LIS	ISS-LIS	|Difference|
Mean Series Count	3.5	3.5	0.1	8.0	7.2	0.8
Mean Group Count	4.9	3.8	1.1	12.0	10.4	1.7
Mean Event Count	9.9	8.8	1.1	55.4	38.0	17.5
Mean Duration	164 ms	161 ms	2.7 ms	266 ms	252 ms	13.8 ms
Mean Extent	5.5 km	6.2 km	0.7 km	5.0 km	4.6 km	0.45 km

875
876

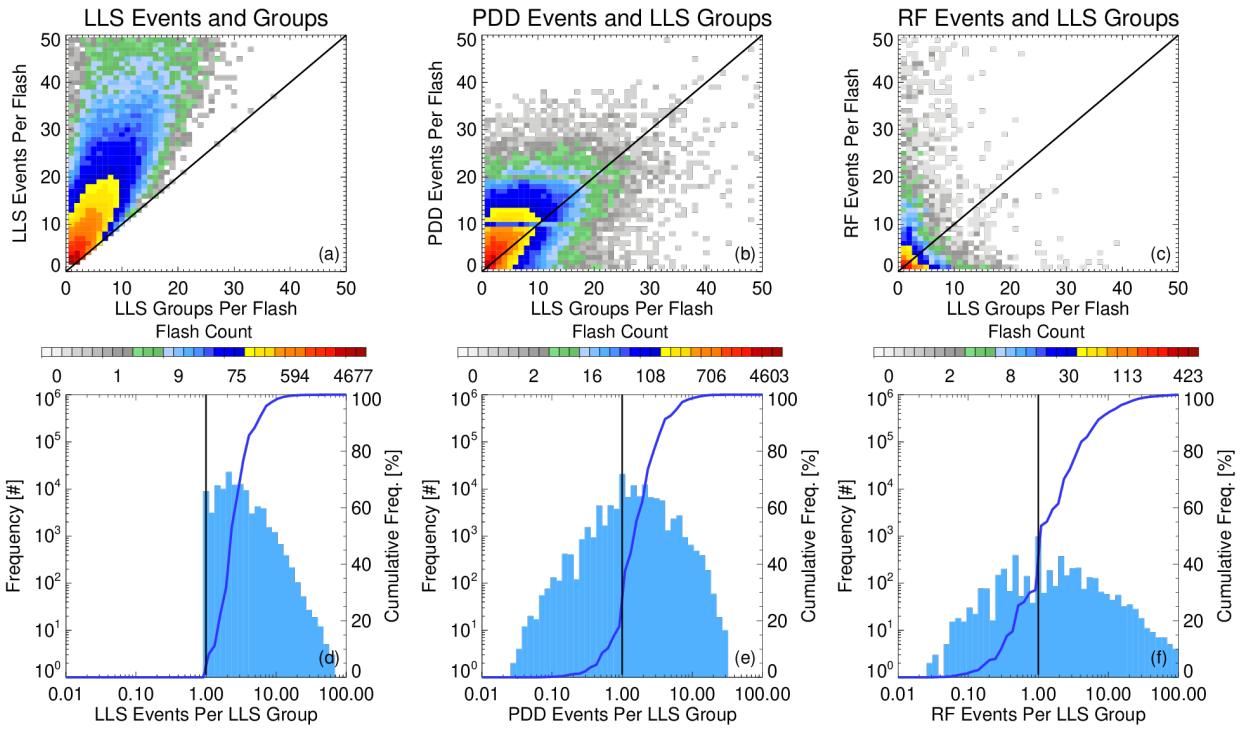

877

878 **Figure 1.** Histograms comparing the numbers of LLS events and LLS groups per flash (a,d), the
879 numbers of PDD events and LLS groups (b,e), and the numbers of RF events and LLS groups
880 (c,f). The top panels plot each combination of parameters as two-dimensional histograms, while
881 the bottom panels show histograms (bars) and Cumulative Distribution Functions (CFDs: lines)
882 of LLS, PDD, and RF event count per LLS group. Unity is indicated with a solid black line in
883 each plot.

884
885

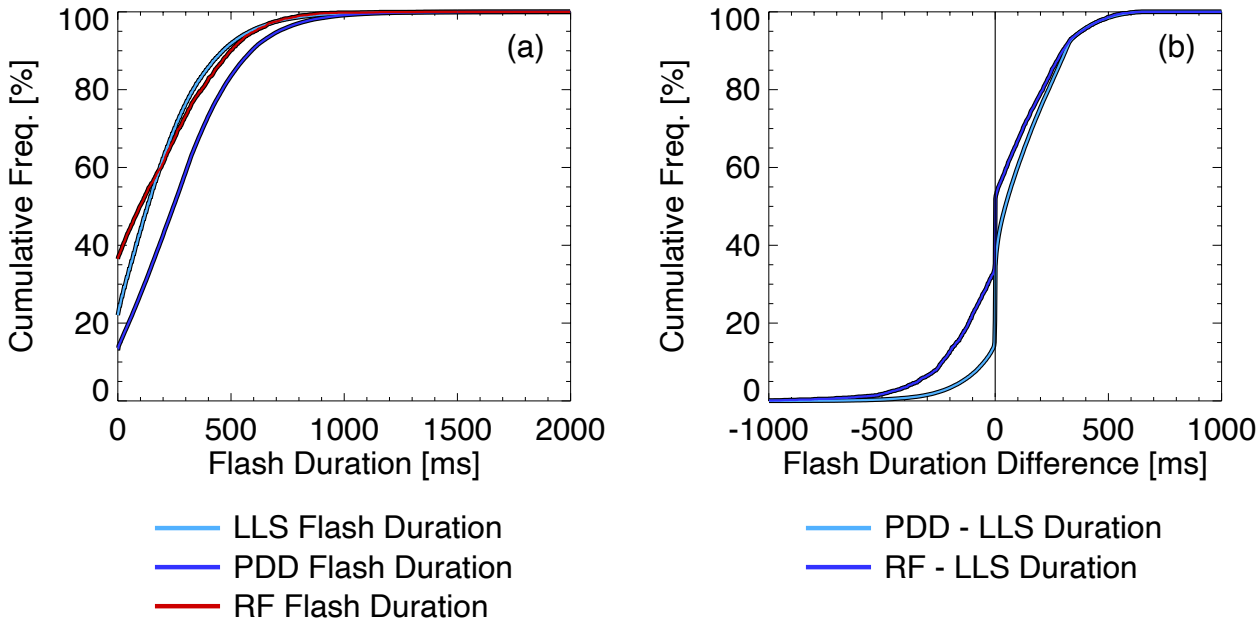

886

887

888 **Figure 2.** CDFs of LLS, PDD, and RF flash duration (a) and differences in the PDD and RF
889 flash duration relative to the LLS flash duration (b).

890

891

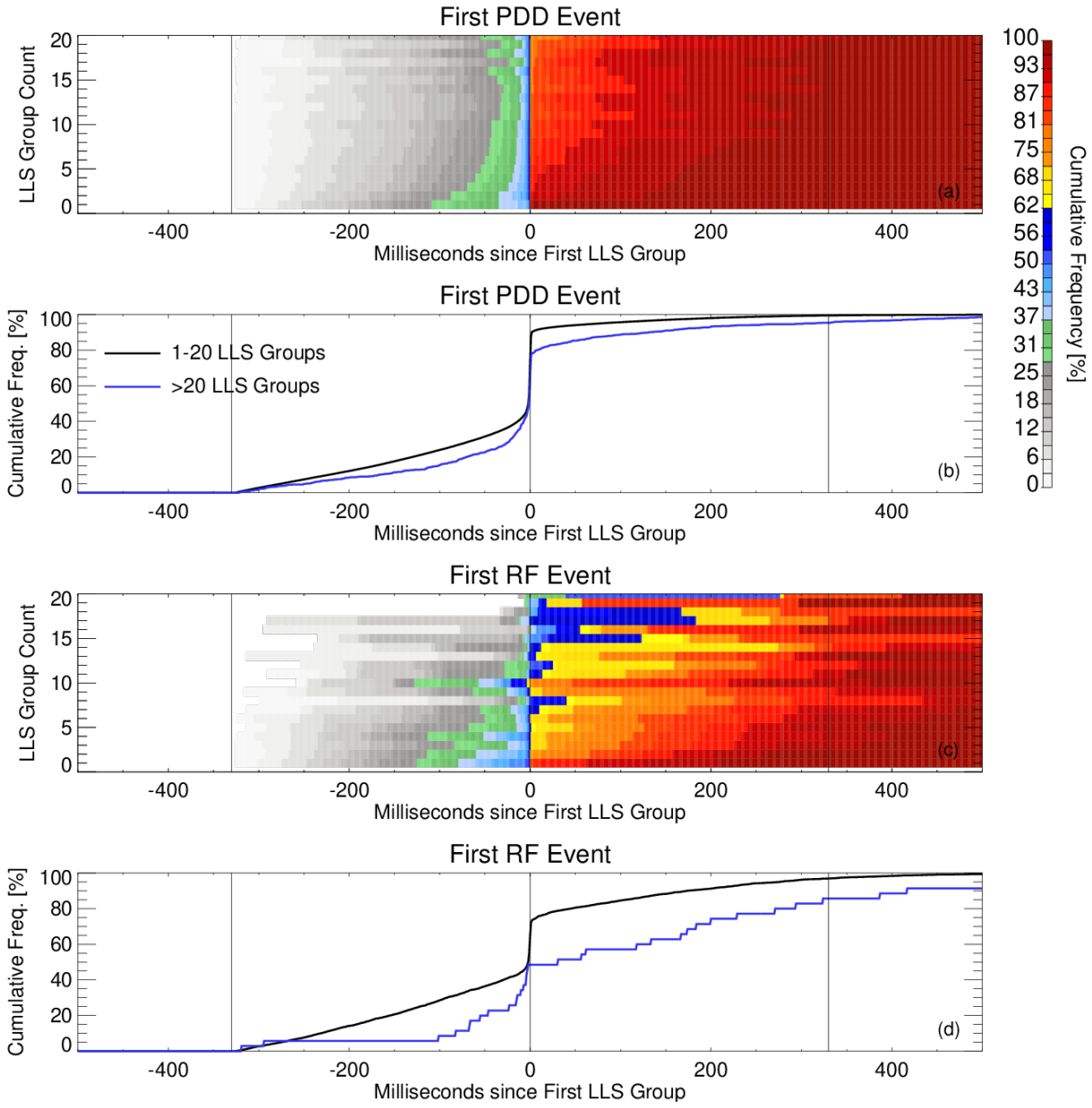

Figure 3. CDFs of the timing of the first PDD (a,b) and RF (c,d) relative to the first LLS group in each flash. The contour plots in (a) and (c) show CDFs for each LLS group count between 1 and 20, while the line plots in (b) and (d) show CDFs for all flashes with 1-20 LLS groups and >20 LLS groups. Solid vertical lines indicate the start of the LLS flash (0 ms) and the extent of the clustering window (±330 ms) for this first LLS group.

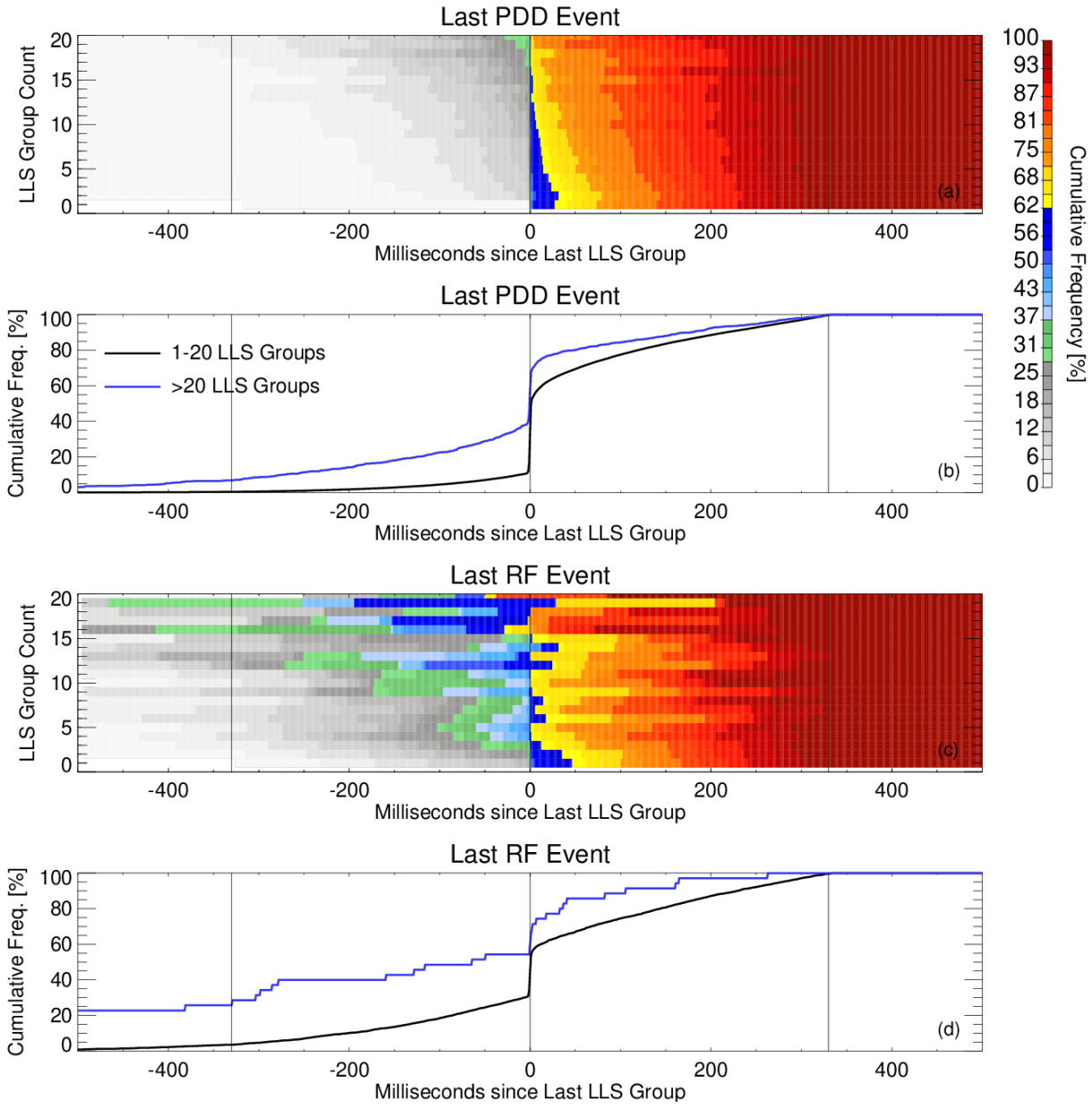

Figure 4. As in Figure 3, but showing CDFs of the timing of the last PDD (a,b) and RF (c,d) triggers relative to the final LLS group in the flash.

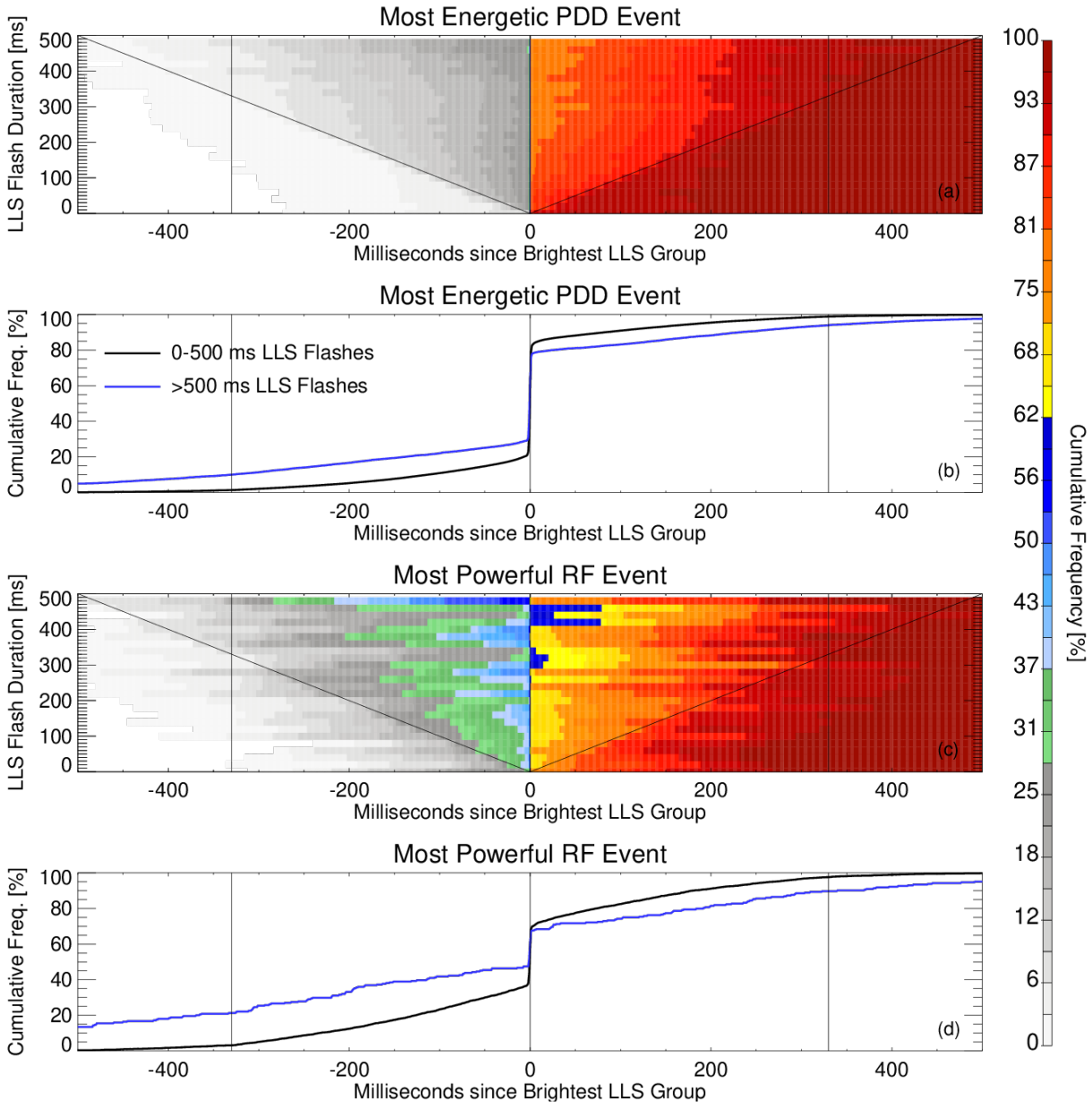

Figure 5. As in Figure 3, but showing CDFs of the timing of the most energetic PDD (a,b) and most powerful RF (c,d) triggers relative to the brightest LLS group in the flash and categorizing flashes by LLS duration rather than group count.

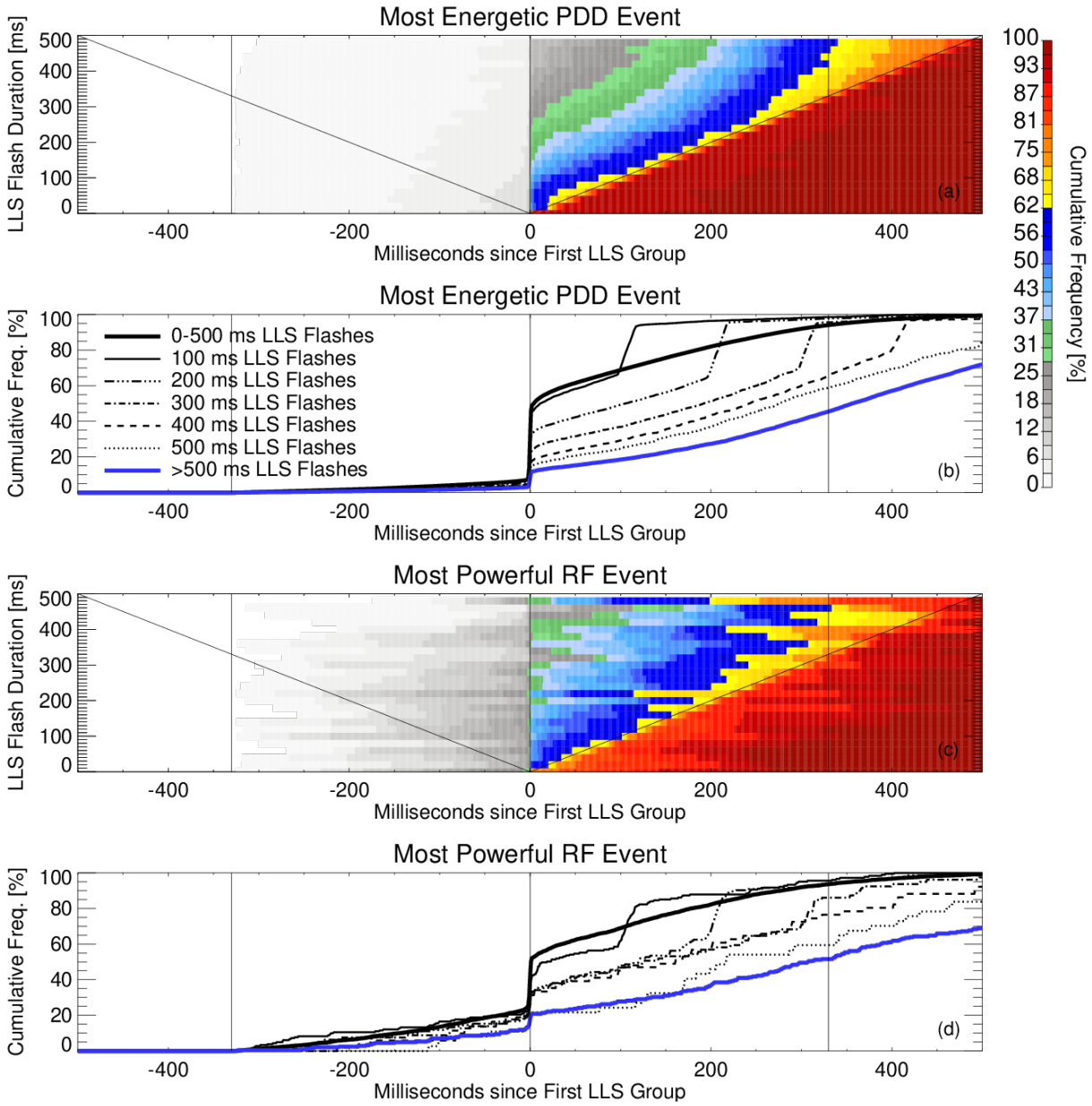

Figure 6. As in Figure 5, but showing CDFs of the timing of the most energetic PDD (a,b) and most powerful RF (c,d) triggers relative to the first LLS group in the flash. Additional curves are added in (b) and (d) for flashes with intermediate durations between 0 and 500 ms.